The High-Precision Solution Structure of *Yersinia* Modulating Protein YmoA Provides Insight into Interaction with H-NS[†]

Robert L. McFeeters,[‡] Amanda S. Altieri,[‡] Scott Cherry,[§] Joseph E. Tropea,[§] David S. Waugh,[§] and R. Andrew Byrd*,[‡]

Structural Biophysics Laboratory and Macromolecular Crystallography Laboratory, Center for Cancer Research, National Cancer Institute, Frederick, Maryland 21702-1201

Received June 19, 2007; Revised Manuscript Received October 2, 2007

ABSTRACT: The high-resolution solution structure of *Yersinia* modulating protein YmoA is presented. The protein is all helical with the first three of four helices forming the central core. Structures calculated with only NOE and dihedral restraints exhibit a backbone root-mean-square deviation (rmsd) of 0.77 Å. Upon refinement against $H^\alpha-C^\alpha$, H^N-N, and $C^\alpha-C'$ *J*-modulated residual dipolar couplings, the backbone rmsd improves to 0.22 Å. YmoA has a high amino acid sequence identity to and a similar overall fold to *Escherichia coli* hemolysin expression modulating protein Hha; however, structural differences do occur. YmoA is also found to be structurally similar to the histone-like nucleoid structuring protein H-NS, indicating that YmoA may intercalate into higher-order H-NS suprastructuring by substituting for an H-NS dimer.

Yersinia pestis, the microorganism responsible for the plague, is a top bioterrorism threat. Left untreated, *Y. pestis*-derived pneumonic infections have a mortality rate of greater than 90%. Administration of antibiotics is an effective countermeasure, but the development of antibiotic resistant strains poses a significant danger. This underscores the need for a better understanding of the microorganism and for alternative therapeutic interventions. One candidate for targeted development of novel treatments against the plague is the *Yersinia* modulating protein YmoA, a suppressor of *Yersinia* virulence factors known to stabilize the H-NS[1] repression complex on the *inv* promoter (*1*).

Knowledge of YmoA function in *Yersinia* has been greatly aided by studies of its *Escherichia coli* homologue hemolysin expression modulating protein, Hha. Repeatedly, YmoA and Hha have been shown to have parallel biological functions in their respective species. The similarity has resulted in YmoA and Hha being described as a new class of bacterial gene expression modulators that act in response to changes in temperature and osmolarity (*2–6*). As an example of their similarity, the *hha* gene can complement *ymoa* mutations of *Yersinia enterocolitica*, provided it is expressed at an adequate level (*7*). Conversely, *ymoa* can complement *hha* mutations in *E. coli* (*8*).

From the parallel biological function of YmoA and Hha, an important common binding partner has been revealed. Initially, *E. coli* Hha was shown to interact with histone-like nucleoid structuring protein H-NS (*9*), a major scaffolding protein in the bacterial nucleoid. The Hha–H-NS complex was found to be responsible for the thermo-osmotic modulation of α-hemolysin expression (*10*). YmoA also interacts with *E. coli* H-NS, a fact used to identify H-NS in *Yersinia* crude cell extracts (*9*). The full-length *Yersinia* and *E. coli* H-NS proteins are greater than 85% identical in amino acid sequence, and the oligomerization domains (to which YmoA and Hha are quite similar) share more than 95% identity. On the basis of the amino acid sequence conservation and parallel function of the Hha–H-NS complex in *E. coli* to the YmoA–H-NS complex in *Yersinia*, the thermo-osmotic regulation of YmoA can also be attributed to the YmoA–H-NS complex.

The roles of H-NS in maintaining bacterial homeostasis and adaptation to environmental stress are well-documented and believed to relate to an architectural suprastructuring of DNA. H-NS participates in structuring of the bacterial chromosome (*11*), in particular chromosomal compaction (*12, 13*). H-NS is known to generate bends in linear duplex DNA (*14*) and was originally thought to bind preferentially to curved DNA (*15*), but with little or no sequence specificity. However, recently, specific high-affinity DNA binding sites have been identified (*16*), and these sites may serve as initiation sites for suprastructuring via H-NS oligomerization. Concentration-dependent higher-order H-NS oligomers (2–20 mers) have been observed (*17*), although thermodynamic data suggest that H-NS predominantly forms tetramers (*18*). Oligomerization is not required for interactions of H-NS with DNA; however, this property has been suggested to be essential for its architectural function (*19*).

H-NS is composed of an N-terminal dimerization domain (residues 1−64), a central region involved in oligomerization (residues 65−89), and a C-terminal DNA binding domain (residues 90−136) (*14, 20, 21*). There are no structural data for the full H-NS protein, but there is information about individual domains, including a high-resolution structure of the DNA binding domain (*22*). Studies of the oligomerization domain (residues 1−89) showed that truncation at residue 64, 57, or 46 results in the formation of only dimers at low concentrations. Hence, we will refer to the initial 64 residues as the dimerization domain. Structures were reported for two forms of the shortened dimerization domain. H-NS residues 1−57 form a head-to-head dimer (*23*), whereas residues 1−46 form an interwoven head-to-tail dimer (*24*). No structural information of higher-order H-NS oligomers is available, yet evidence for a head-to-tail arrangement of homodimers has been presented (*23*). Although no structure of the Hha−H-NS complex has been reported, recent studies have characterized the residues on both Hha and the N-terminal H-NS domain that are involved in binding (*25, 26*). Also, substitution of Hha for the N-terminal oligomerization domain of H-NS is able to rescue some *hns* phenotypes (*27*). On the basis of the amino acid sequence similarity, the same is assumed to hold for YmoA. These results suggest a homologous function for YmoA or Hha and the H-NS oligomerization domain; however, until now, the high-resolution structural support for this postulation has been absent.

Herein, we present the solution structure of YmoA and examine its relationship to the H-NS oligomerization domain and the YmoA−H-NS interaction. We demonstrate that YmoA shares significant regions of similar structure with the oligomerization domain of H-NS, which provides experimental support for the hypothesis that YmoA or Hha should be thought of as an independent oligomerization domain of H-NS (*9*). The structural comparison also indicates that YmoA could substitute for an entire H-NS dimer. The improved understanding of YmoA and its relationship with H-NS helps explain their related biological function.

EXPERIMENTAL PROCEDURES

Cloning, Expression, and Purification of YmoA-His₆. The open reading frame encoding YmoA was amplified from *Y. pestis* genomic DNA (strain 195/P) by polymerase chain reaction (PCR) using the following oligonucleotide primers: 5′-GAG AAC CTG TAC TTC CAG GGT ACA AAA ACT GAC TAC CTG ATG CGT TTA AG-3′ and 5′-ATT AGT GAT GAT GGT GGT GAT GTT TCA CAT GTT GCC ATA CAG TAG GTG-3′. This PCR amplicon was subsequently used as the template for a second PCR with the following primers: 5′-GGG GAC AAG TTT GTA CAA AAA AGC AGG CTC GGA GAA CCT GTA CTT CCA G-3′ and 5′-GGG GAC CAC TTT GTA CAA GAA AGC TGG GTT ATT AGT GAT GAT GGT GGT GAT G-3′. The amplicon from the second PCR was inserted by recombinational cloning into the pDONR201 entry vector (Invitrogen, Carlsbad, CA) to create pKM970, and the nucleotide sequence of the entire insert was confirmed experimentally. The open reading frame encoding YmoA, now bracketed by a hexahistidine tag on its C-terminus and a recognition site (ENLYFQG) for tobacco etch virus (TEV) protease on its N-terminus, was moved by recombinational

cloning from pKM970 into the pKM596 destination vector (*28*) to construct pKM974. pKM596, a derivative of pMal-C2 (New England Biolabs, Beverly, MA), was designed to produce recombinant proteins as in-frame fusions to the C-terminus of *E. coli* maltose-binding protein (MBP). Therefore, pKM974 directed the expression of YmoA in the form of an "affinity sandwich" with MBP fused to its N-terminus and a hexahistidine tag joined to its C-terminus. The MBP moiety could be removed by cleaving the fusion protein with TEV protease at a designed site in the linker to yield a recombinant YmoA with a single non-native glycine residue on its N-terminus and a hexahistidine tag on its C-terminus.

The MBP−YmoA-His₆ fusion protein was overproduced in *E. coli* BL21(DE3) cells containing an auxiliary plasmid, pRK603, that constitutively produces the catalytic domain of TEV protease (*29*). The fusion protein was cleaved in vivo to generate YmoA with a C-terminal hexahistidine tag. Cells were grown to mid-log phase (OD₆₀₀ ∼ 0.5) at 37 °C in M9 minimal salts containing 0.2% [¹³C]glucose (Spectra), 0.1% ¹⁵NH₄Cl (Spectra), trace metals, vitamin B complex, 100 μg/mL ampicillin, and 35 μg/mL kanamycin. Overproduction of the fusion protein was induced by the addition of 1 mM isopropyl-β-D-thiogalactopyranoside for 4 h at 30 °C. The cells were pelleted by centrifugation and stored at −80 °C.

All procedures were performed at 4 °C. *E. coli* cell paste was suspended in ice-cold 50 mM sodium phosphate (pH 8) and 300 mM NaCl buffer (buffer A) containing Complete EDTA-free protease inhibitor tablets (Roche Molecular Biochemicals, Indianapolis, IN) and disrupted with an APV Gaulin model G1000 homogenizer at 10 000 psi. The homogenate was centrifuged at 30000*g* for 30 min, and the supernatant was filtered through a 0.45 μm cellulose acetate membrane and applied to a 10 mL Ni-NTA superflow column (Qiagen, Valencia, CA) equilibrated in buffer A. The column was washed with buffer A containing 25 mM imidazole, and bound protein was eluted with a 25 to 200 mM imidazole gradient over 10 column volumes. Fractions containing recombinant protein were pooled, concentrated using a YM-3 membrane (Millipore, Billerica, MA), and fractionated on a HiPrep 26/60 Sephacryl S-100 HR column (Amersham Biosciences, Piscataway, NJ) equilibrated with buffer A. Fractions containing YmoA-His₆ were pooled, dialyzed against 50 mM sodium phosphate (pH 6), 150 mM NaCl, and 5 mM dithiothreitol buffer, and concentrated to 1.5 mM (determined spectrophotometrically using a molar extinction coefficient of 10 810 M⁻¹ cm⁻¹). The final product was judged to be >95% pure by SDS−PAGE. The molecular weight was confirmed by electrospray mass spectroscopy indicating a degree of ¹³C/¹⁵N incorporation of >98%.

NMR Spectroscopy. All data were collected at 25 °C on Varian Inova spectrometers. Assignment data were collected at 600 MHz, NOESY and ¹⁵N T_1/T_2 data at 800 MHz, and RDC data at 500 MHz. Experiments used for backbone resonance assignment included two-dimensional (2D) ¹⁵N- and ¹³C-HSQC and three-dimensional (3D) HNCACB, CBCACONH, and HNCO experiments. HCCONH and HCCH-TOCSY experiments were used to determine a bulk of the side chain assignments (*30*). Aromatic side chain assignments were determined from 2D C^β−H^δ and C^β−H^ϵ correlation experiments and a 3D TROSY-type HCCH
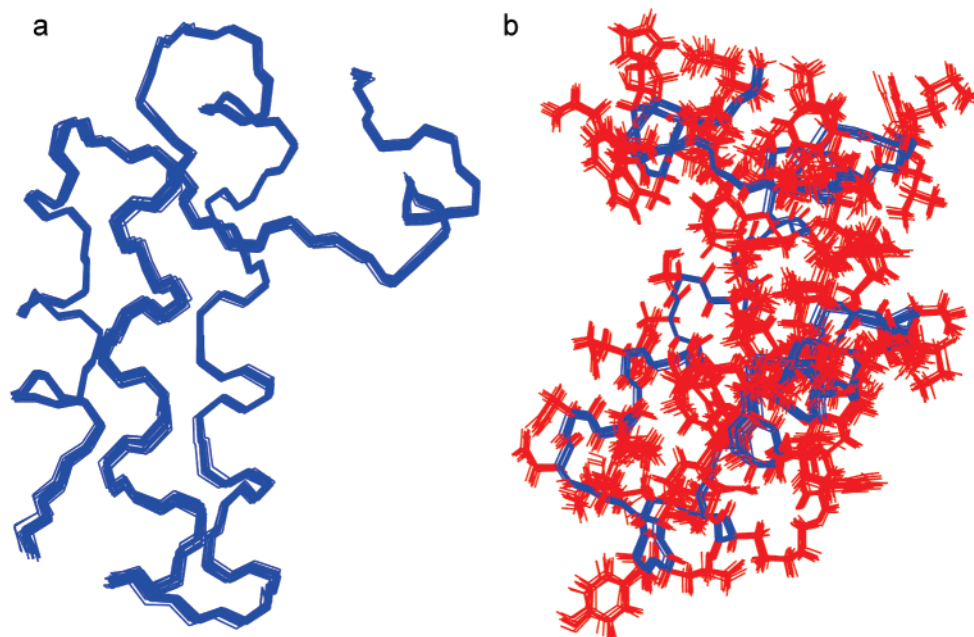
FIGURE 1: Solution structure of YmoA. (a) Overlay of the backbone trace from the 20 lowest-energy structures after refinement against $H^\alpha-C^\alpha$, H^N-N, and $C^\alpha-C'$ RDCs. (b) Overlay of the same 20 structures with side chains included in red. The scale is ∼80% of panel a.

experiment (*31−33*). NOE data were derived from a 3D ^{13}C-edited NOESY experiment with a 100 ms mixing time and 3D ^{15}N-edited NOESY with a 130 ms mixing time. Sweep widths for the ^{13}C-edited experiment were 8292 Hz for both ^{1}H dimensions and 4020 Hz for the ^{13}C dimension. The ^{1}H carrier was set to the water (4.77 ppm) and the ^{13}C carrier to 43 ppm, and 128 × 32 × 1024 complex points were collected. For the ^{15}N-edited experiment, the indirect ^{1}H and ^{15}N sweep widths were 6400 and 1300 Hz, respectively, whereas the direct ^{1}H sweep width was 8385 Hz. The ^{1}H carrier was again set to water and the ^{15}N carrier to 119 ppm. A data matrix of 70 × 22 × 1280 complex points was collected. $^{3}J(H^N-H^\alpha)$ coupling constants were obtained from an HNHA experiment (*34*). $H^\alpha-C^\alpha$, H^N-N, and $C^\alpha-C'$ RDCs were measured using *J*-modulated experiments (*35*) in a stretched 6% polyacrylamide gel alignment medium (*36, 37*). All spectra were processed with nmrPipe (*38*) and analyzed using Sparky (*39*). ^{15}N T_1 and T_2 data were collected and analyzed as described previously (*40, 41*).

Structural Restraints and Calculation. NOE-based distance restraints were determined from manually peak picked and assigned spectra. Peak heights derived from Sparky were used to bin NOEs into five categories, corresponding to distance restraints of 2.2 +0.4/−1.0, 2.8 +0.5/-1.4, 3.8 +0.6/−1.8, 5.2 +0.6/−2.8, and 6.0 +1.2/−3.2 Å. Well-resolved resonances with known stereochemistry were used to validate and calibrate the binning procedure. ϕ and ψ dihedral angle constraints were derived from chemical shift data using TALOS (*42*). RDCs were determined from the difference in couplings measured from gel-aligned and isotropic samples. The initial structure calculation, using only NOE and dihedral restraints, was performed by a simulated annealing algorithm in XPLOR-NIH starting from an extended conformation (*43*). The structure nearest the average was then used as input coordinates for refinement against $H^\alpha-C^\alpha$, H^N-N, and $C^\alpha-C'$ residual dipolar couplings. A final ensemble of 200 structures was then calculated using

the extended python functionality incorporated into XPLOR-NIH (*43*).

Data Bank Accession Numbers. Chemical shift assignments and experimental restraints have been deposited in the BioMagResBank as entry 15486. Coordinates for the 20 lowest-energy structures of YmoA have been deposited in the RCSB Protein Data Bank as entry 2JVP.

RESULTS

More than 96% of the backbone ^{1}H, ^{15}N, $^{13}C'$, and $^{13}C^\alpha$ NMR resonances of YmoA were assigned from a battery of triple-resonance experiments. Also, nearly 95% of the side chain resonances were assigned, with special attention paid to aromatic residues. The completeness of assigned resonances resulted in the structure calculation accounting for all but 53 of 2219 NOE cross-peaks from a manually peak picked ^{13}C-edited NOESY spectrum. A ^{15}N HSQC is included in the Supporting Information to illustrate the high quality of the NMR data. The backbone root-mean-square deviation (rmsd) from the mean for all residues except the hexahistidine tag (1−67) for the 20 lowest-energy structures of 200 calculated was 0.77 ± 0.19 Å. After refinement against 52 H^N-N, 51 $H^\alpha-C^\alpha$, and 38 $C^\alpha-C'$ *J*-modulated residual dipolar couplings, a backbone rmsd of 0.22 ± 0.11 Å was obtained for the 20 lowest-energy structures. The ensemble of final structures is shown in Figure 1. A summary of the experimental restraints is given in Table 1, and a normalized distribution of gel-aligned RDCs with calculated versus observed plots is included as Supporting Information. The ^{15}N relaxation rates, also included as Supporting Information, show only a moderate change (≤10%) in T_1, T_2, and T_1/T_2 in the loops and turns. Thus, there is evidence for well-defined structure in the loops, supporting the extremely low rmsd. A calculated τ_c value of 5.6 ns fits the expected value for monomeric YmoA.

Structure of YmoA. YmoA is a 67-residue, all-helical protein, in agreement with ϕ and ψ torsion angles predicted

Table 1: Summary of Structure Statistics

resonances assigned (%)	
backbone	96.9
side chain[a]	94.6
no. of NOE constraints[b]	
intraresidue ($i = j$)	1322
sequential ($\|i - j\| = 1$)	313
medium-range ($1 < \|i - j\| < 5$)	262
long-range ($\|i - j\| > 5$)	171
total	2068
NOEs per residue	30.9
inter-residue NOEs per residue	11.1
dihedral constraints (Φ:Ψ)	51:51
residual dipolar couplings $H^\alpha-C^\alpha$, H^N-N, $C^\alpha-C'$	52, 51, 38

	NOE	RDC refined
no. of distance violations[c]		
NOE violations >0.55 Å per structure	2	20
average violation >0.55 Å (Å)	0.804	0.842
dihedral angle violations[c]		
dihedral violations >5° per structure	0	4
average violation >5° (deg)	0	7.1
average rmsd (Å)[d]		
backbone atoms (N, C^α, C')	0.77 ± 0.19	0.22 ± 0.11
heavy atoms	1.24 ± 0.16	0.30 ± 0.13
Ramachandran summary (%)		
most favored regions	49	45
additionally allowed regions	10	14
generously allowed regions	3	4
disallowed regions	1	0

[a] The following resonances were not considered to be routinely assignable: Lys NH^{3+}, Arg NH_2, Cys SH, Ser/Thr/Tyr OH, Pro N, C-terminal carbonyl, side chain carbonyl, and aromatic nonprotonated carbon atoms. [b] Does not include ambiguous NOEs that could belong to more than one class. [c] Only the structured region (residues 2−66) considered for rmsd and dihedral violations. [d] Average rmsd from the mean and one standard deviation reported.

from chemical shifts using TALOS (*42*). The overall protein shape is an oblate, hemi-ellipsoid having a major axis (radial) of 27 Å and a minor axis (height) of 19 Å. Four helices are defined by residues 2−12, 17−27, 32−50, and 60−64 and are designated helices 1−4, respectively. The core structure of YmoA is a helical bundle comprised of helices 1−3. The structure is stabilized by a contiguous hydrophobic interface involving residues L7 and L10 from helix 1, I16, L19, and I23 from helix 2, L30 from the turn between helix 2 and helix 3, and L35, F38, A42, and L46 from helix 3. Helix 4 is the shortest helix and is positioned against the outer face of the C-terminal end of helix 3. It is connected to the core three-helix bundle by hydrophobic interactions involving V62 and W63 of helix 4 and A47 of helix 3 and I58 in the loop between helix 3 and helix 4. The secondary structure of helix 4 is well-defined by numerous sequential and intraresidue NOEs. RDC refinement did not change the average position of helix 4 with respect to the core but did significantly improve the precision of the orientation.

Comparison to Hha Structure. YmoA and its *E. coli* homologue Hha share 75% amino acid sequence identity and 83% sequence similarity. The structure of Hha (PDB entry 1JW2) was determined as part of a structural proteomics effort (*44*). The overall shape and elements of secondary structure (Figure 2) are conserved between YmoA and Hha, as expected from the high degree of sequence similarity. However, structural differences do exist. Alignment of the first two helices yields a backbone rmsd of 0.98 Å, whereas including helix 3 increases the rmsd to 1.5 Å. The differences

in interhelical angles between YmoA and Hha are 1.7° for the angle between helices 1 and 2, 6.1° for the angle between helices 1 and 3, and 13° for the angle between helices 2 and 3. Another difference is a kink in helix 3 of YmoA, which is not observed in Hha. The kink is initially observed in the NOE-only structure and remains in the final structure following RDC refinement. Also, there is a difference in surface charge distribution between YmoA and Hha (Figure 2b), which is due to the presence of acidic residues D33 and E36 in YmoA that are positionally equivalent to N38 and A41 in Hha.

The most noticeable difference between YmoA and Hha is the orientation of helix 4. When core helices 1−3 are aligned, the angle between the axis of helix 4 in YmoA versus Hha is roughly 50°. This reorientation appears to be caused by significant torsion angle differences for YmoA residues 53 and 56 compared to the equivalent residues in Hha and by the additional proline, P60 in YmoA, substituting for S65 in Hha. NOE and ^{13}C chemical shift data (*45*) indicate that both P59 and P60 in YmoA are in the trans configuration with no evidence of cis−trans isomerization. P64 in Hha, equivalent to P59 in YmoA, is reported in the trans configuration (*44*). In the NOE-only structure of YmoA, the orientational precision of helix 4 is lower than that of helices 1−3. The Hha structure also indicates a lower precision for helix 4. However, the precision of helix 4 in the final structure of YmoA is significantly improved following RDC refinement. It is not possible to know whether the same situation would hold for Hha if RDC data were available.

Similarity to the H-NS Oligomerization Domain. YmoA shares only moderate amino acid sequence similarity (33%) with the oligomerization domain of H-NS; however, significant structural similarity exists (Figure 3). First, considering the H-NS dimerization domain, two different configurations have been reported (*23, 24*), but the H-NS monomer structure is nearly identical in both. Superposition of YmoA helices 1 and 2 with H-NS monomer helices 2h and 3h (H-NS helices are followed with an h to distinguish them from helices of YmoA) yields a backbone rmsd of 1.8 Å, indicating significant structural similarity. H-NS residues preceding helix 2 were omitted from the superposition, since they do not contribute to dimerization (*23*). From this alignment, the position of important residues is preserved between YmoA and the dimerization domain of H-NS. For example, R14, a key functional residue in H-NS, structurally aligns with R11 of YmoA. Moreover, the abundant negative charge found on helix 3h of H-NS is retained by helix 2 of YmoA. Specifically, residues E23, E26, E30, and K31 of H-NS structurally align with D17, E20, E24, and K25 of YmoA, respectively (Figure 3b). All of these exposed, charged residues are also conserved in Hha, as well as the known H-NS paralogs StpA and Sfh. Also, the side chain position of the single cysteine residue present in YmoA, Hha, and the N-terminal dimerization domain of H-NS is preserved. These conserved side chain properties and the backbone structure emphasize the similarity of YmoA helices 1 and 2 to the dimerization domain of H-NS.

The comparison of YmoA or Hha to H-NS can be extended to the full oligomerization domain. When YmoA helices 1 and 2 are aligned with helices 2h and 3h in one molecule of either H-NS dimer structure, helix 3 of YmoA
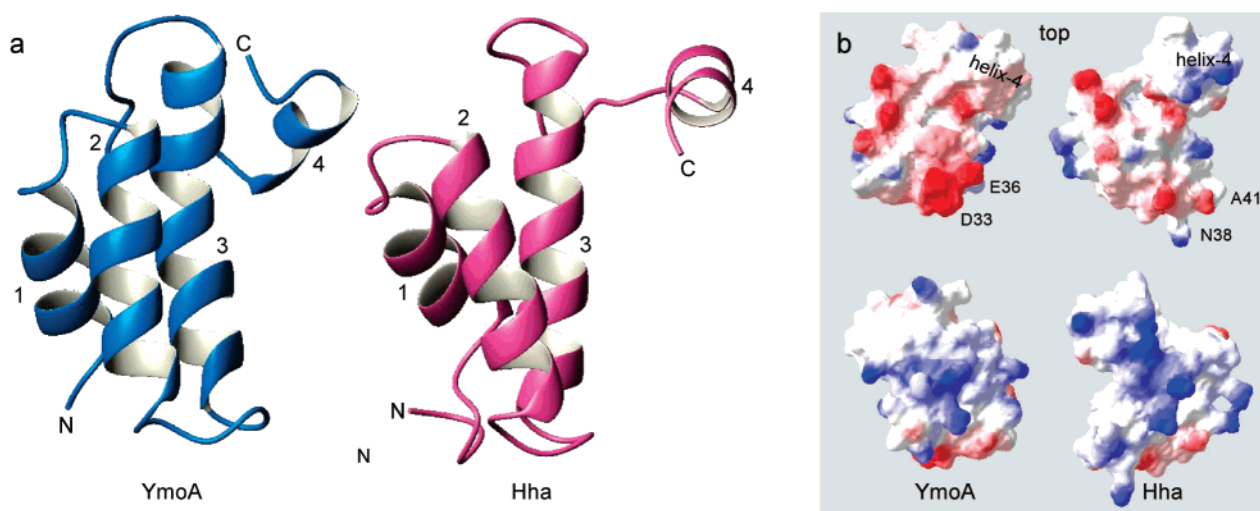
FIGURE 2: Comparison of YmoA to Hha. (a) Side-by-side comparison of YmoA and Hha structures, aligned by the three core helices. The orientation chosen shows that helix 4, at the top right of each structure, is positioned quite differently. Also, changes near the C-terminal end of helix 2 and the N-terminal of helix 3 are evident. (b) Electrostatic surface plots of YmoA and Hha showing the large negative charge introduced by changing N38 and A41 in Hha to D33 and E36 in YmoA, respectively.
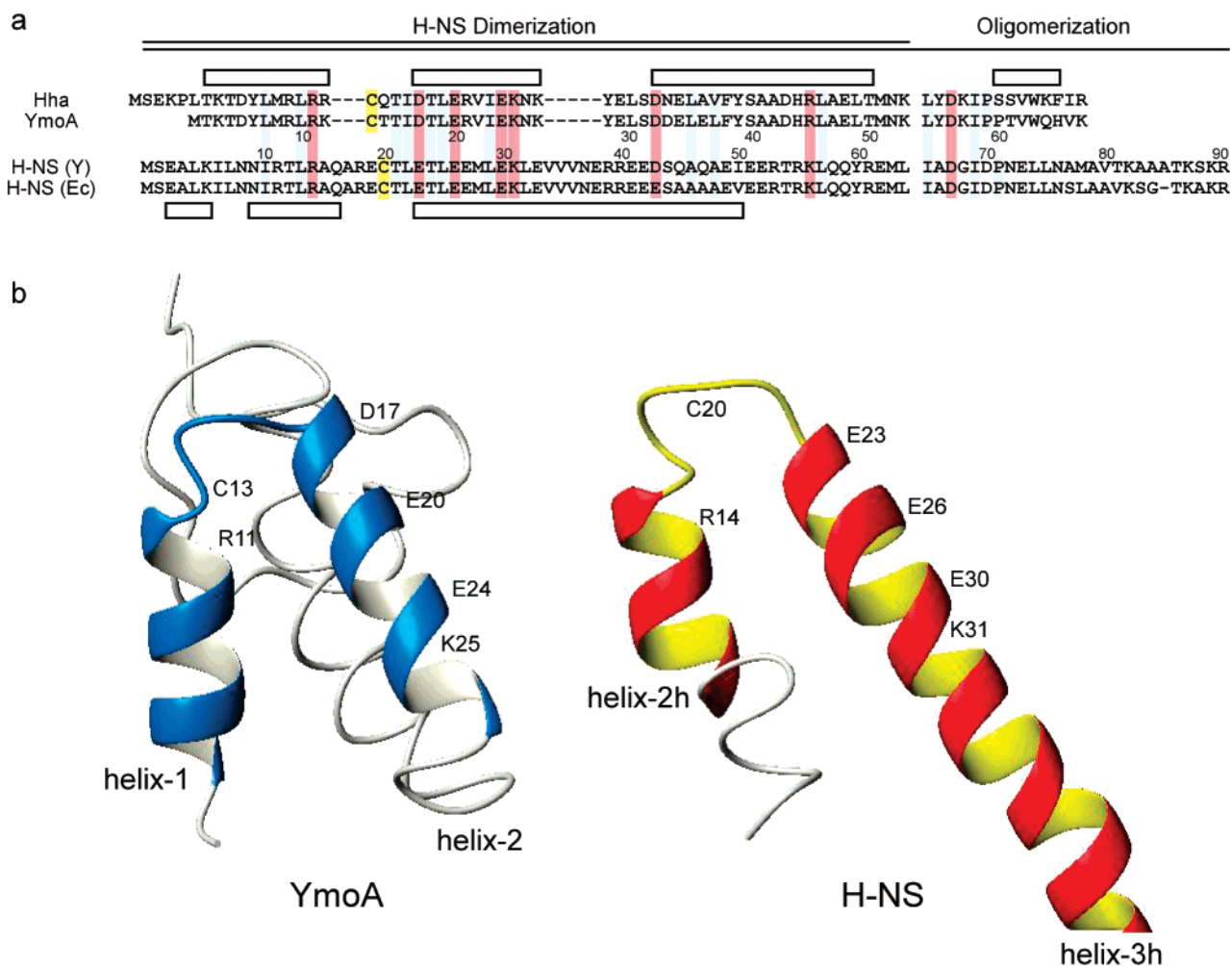

FIGURE 3: Structural similarity to H-NS. (a) Structure-based sequence alignment of Hha, YmoA, and H-NS from *Y. enterocolitica* and *E. coli*. Conserved charged residues are shaded in red, other conserved residues in gray, and the lone cysteines in yellow. Helices are shown as boxes above the sequence for YmoA and Hha and below for H-NS. (b) Ribbon diagrams of YmoA and H-NS helices 2h and 3h exhibit structural similarity. Residue labels indicate the position of conserved charged residues and the lone cysteine.

occupies a position similar to that of helix 3h in the *other* H-NS molecule of the H-NS dimer, denoted as helix 3h′ (Figure 4). In this configuration, helix 3 of YmoA occupies

a majority of the space required by the second H-NS monomer. Therefore, if YmoA substituted for an H-NS oligomerization domain within a growing H-NS scaffold,
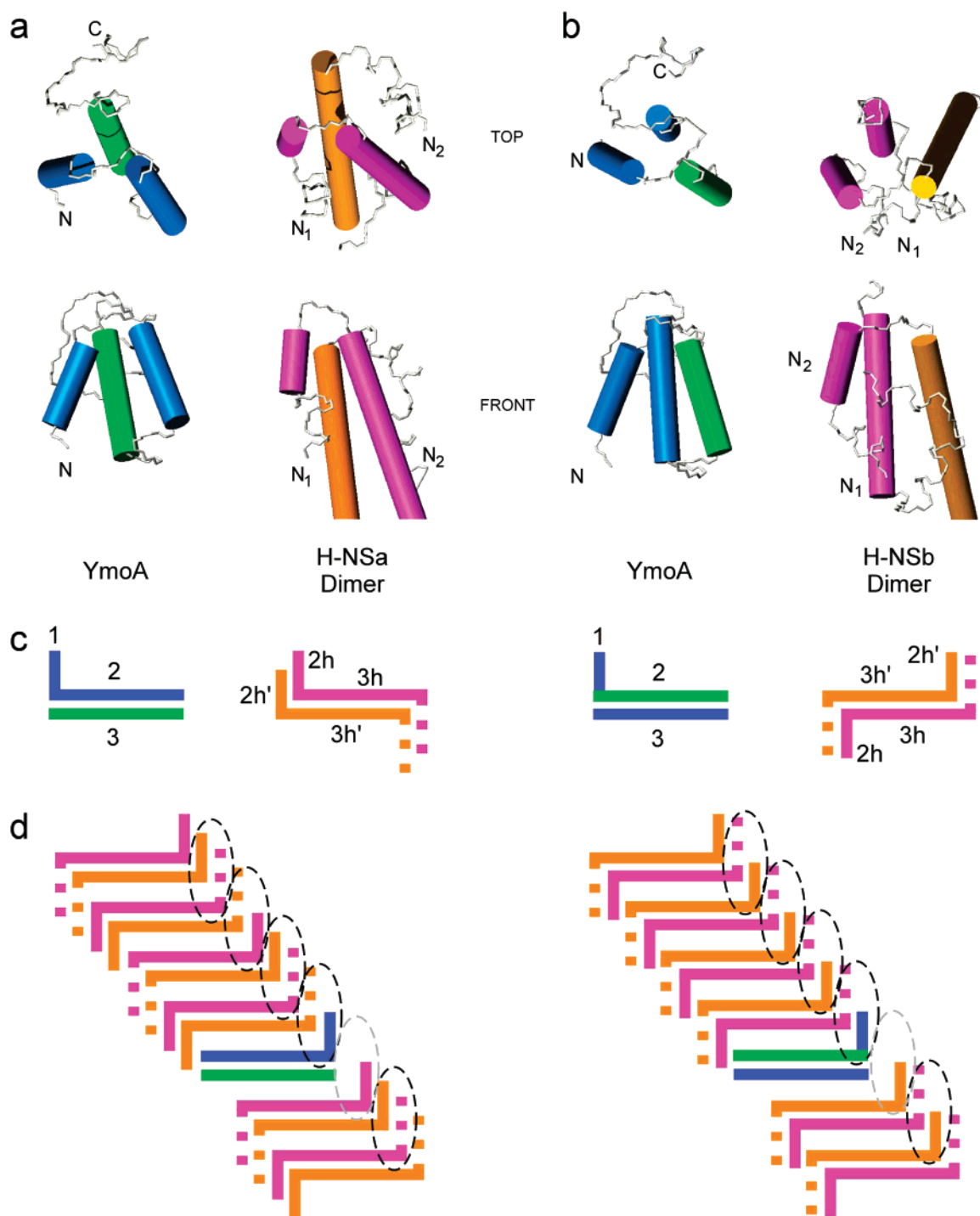
FIGURE 4: Potential role for YmoA substitution of an H-NS dimer. Structures of YmoA and the different H-NS dimers are shown where helices are replaced by cylinders, aligned along helical axes. (a) Alignment of YmoA with the head-to-head H-NS oligomerization domain dimer (*22*) (H-NSa, PDB entry 1LR1). Helices 1 and 2 (blue) match helices 2h and 3h (magenta). Helix 3 (green) occupies a majority of the space from helix 3h′ (orange) of the second monomer. (b) Alignment of YmoA with the head-to-tail interwoven H-NS oligomerization domain dimer (*23*) (H-NSb, PDB entry 1NI8). Helices 1 and 3 (blue) match helices 2h and 3h′ (magenta). Helix 2 (green) occupies a majority of the space from helix 3h (orange). (c) Line representation of the helices in YmoA and the H-NS oligomerization domain, colored as in panel a. Helices are numbered. (d) Schematic diagram proposing models for incorporation of YmoA into the H-NS scaffold: (left) YmoA is incorporated into the head-to-head H-NSa dimer, and (right) YmoA is incorporated into the head-to-tail interwoven dimer. The dashed ovals indicate proposed oligomerization interfaces (*22*). Note that regardless of H-NS dimerization structure, the overall YmoA interactions are the same.

then YmoA could sterically block other H-NS molecules from binding. This role suggests that YmoA could substitute for an H-NS dimer, and higher-order oligomerization could still be possible, albeit altered. Support for YmoA or Hha mimicking an H-NS dimer comes from several points. First, sequence alignment shows that residues from helix 4 (59–

67 in YmoA and 64–72 in Hha) align with H-NS residues 65–73 that are required for higher-order oligomerization. Second, H-NS residues following P71 are predicted to form a helix, directly analogous to P60 and P64 followed by helix 4 in YmoA and Hha, respectively. Third, it has been shown that perturbation of the C-terminus of Hha abrogates binding

to H-NS (*9*), and Hha residues in helix 4 exhibit changes upon binding to H-NS (*25*). Thus, the residues important for binding of YmoA and Hha to H-NS are directly related to those involved in oligomerization of H-NS.

DISCUSSION

YmoA and Hha exhibit structural differences, despite their amino acid sequences being >83% similar. Minor changes in the core three-helix bundle are attributed to differences in the loop between helix 2 and helix 3 and a kink in helix 3 of YmoA, which is not observed in Hha. As illustrated in panels a and b of Figure 2, the most notable difference between YmoA and Hha is the position and orientation of helix 4. This alteration is most likely a consequence of replacing residue S65 of Hha with P60 in YmoA, yielding an all-trans, diproline motif (P59–P60). The uniformity of ^{15}N relaxation parameters observed for the residues in the linker and helix 4 of YmoA indicates that helix 4 is in a stable conformation. The use of RDC data to refine the structure of YmoA may indicate that the difference may be due to more extensive restraints and not a species or functional difference. Hence, it is reasonable to interpret interactions of either Hha or YmoA on the basis of the structure presented here.

YmoA shows significant similarity to the N-terminal oligomerization domain of H-NS, as previously suggested on the basis of amino acid sequence (*9*). YmoA helices 1 and 2 superimpose with H-NS monomer helices 2h and 3h, conserving the position of charged residues. The similarity of YmoA and Hha sequences and structures to those of H-NS extends beyond the dimerization domain. Residues 65–89, important for higher-order H-NS oligomerization (*17*, *23*), correspond to C-terminal YmoA and Hha residues that exhibit changes in the Hha–H-NS interaction (*25*). This agrees with biochemical evidence from *E. coli* where perturbation of the C-terminus of Hha prevents formation of the Hha–H-NS complex (*9*). Similarly, H-NS oligomerization is known to be dependent on electrostatic interactions (*18*) as is the interaction between YmoA and H-NS (*9*). This commonality, along with the structural preservation of charged residues, supports the functional similarity of YmoA to the oligomerization domain of H-NS and likens the YmoA–H-NS interaction to the H-NS dimer–dimer interaction. It also suggests that YmoA may substitute for H-NS in an osmotically dependent fashion, providing a straightforward explanation for osmotic regulation by YmoA. Although structures of the Hha–H-NS complex or the H-NS–H-NS oligomer are not known, it appears that YmoA may structurally substitute for an entire H-NS dimer in a higher-order structuring, not simply supplanting a single H-NS monomer. This substitution could lead to altered scaffolding and altered DNA suprastructuring.

YmoA regulates the expression of virulence factors and interacts with one of the most abundant histone-like nucleoid structuring proteins. For example, YmoA stabilizes the H-NS promoter repression complex for the primary invasion factor *inv* (*1*, *46*), suggesting that the YmoA–H-NS interaction could be a good target for anti-*Yersinia* therapeutics. A drug or biological mimetic that blocked the YmoA–H-NS interaction could potentially be used to alter suprastructuring and thus impact the expression profile of the organism. Fine-

tuning such expression profile management could lead to altered virulence of the organism. The uniqueness of this regulatory system to bacteria provides the potential for selectivity. Further knowledge of the YmoA–H-NS interaction will be critical to development of such a therapeutic.

In conclusion, the high-resolution solution structure of YmoA provides significant insight into the emerging biological function of this protein. The structural conservation of YmoA and the oligomerization domain of H-NS goes beyond a sequence alignment and solidifies the existing idea that YmoA should be considered an independent oligomerization domain of H-NS. The conserved features between YmoA or Hha and the N-terminal domain of H-NS provide an explanation for why a chimeric H-NS protein constructed by substituting Hha for the H-NS oligomerization domain compensates for some *hns*-induced phenotypes (*27*). Substitution of YmoA into the H-NS scaffold could alter DNA suprastructuring and provide a means for YmoA to regulate transcription. These findings open the door to further study, including structure–function studies of the YmoA–H-NS complex and targeted development of anti-*Yersinia* therapeutics.

ACKNOWLEDGMENT

SUPPORTING INFORMATION AVAILABLE

^{15}N-HSQC spectra of YmoA, RDC distribution and cross validation, and relaxation parameters. This material is available free of charge via the Internet at http://pubs.acs.org.

REFERENCES

1. Ellison, D. W., and Miller, V. L. (2006) H-NS represses inv transcription in *Yersinia enterocolitica* through competition with RovA and interaction with YmoA, *J. Bacteriol.* *188*, 5101–5112.
2. de la Cruz, F., Carmona, M., and Juarez, A. (1992) The Hha protein from *Escherichia coli* is highly homologous to the YmoA protein from *Yersinia enterocolitica*, *Mol. Microbiol.* *6*, 3451–3452.
3. Nieto, J. M., Carmona, M., Bolland, S., Jubete, Y., de la Cruz, F., and Juarez, A. (1991) The hha gene modulates haemolysin expression in *Escherichia coli*, *Mol. Microbiol.* *5*, 1285–1293.
4. Carmona, M., Balsalobre, C., Munoa, F., Mourino, M., Jubete, Y., De la Cruz, F., and Juarez, A. (1993) *Escherichia coli* hha mutants, DNA supercoiling and expression of the haemolysin genes from the recombinant plasmid pANN202-312, *Mol. Microbiol.* *9*, 1011–1018.
5. Cornelis, G. R., Sluiters, C., Delor, I., Geib, D., Kaniga, K., Lambert de Rouvroit, C., Sory, M. P., Vanooteghem, J. C., and Michiels, T. (1991) ymoA, a *Yersinia enterocolitica* chromosomal gene modulating the expression of virulence functions, *Mol. Microbiol.* *5*, 1023–1034.
6. Mourino, M., Madrid, C., Balsalobre, C., Prenafeta, A., Munoa, F., Blanco, J., Blanco, M., Blanco, J. E., and Juarez, A. (1996) The Hha protein as a modulator of expression of virulence factors in *Escherichia coli*, *Infect. Immun.* *64*, 2881–2884.

7. Mikulskis, A. V., and Cornelis, G. R. (1994) A new class of proteins regulating gene expression in enterobacteria, *Mol. Microbiol. 11*, 77−86.

8. Balsalobre, C., Juarez, A., Madrid, C., Mourino, M., Prenafeta, A., and Munoa, F. J. (1996) Complementation of the hha mutation in *Escherichia coli* by the ymoA gene from *Yersinia enterocolitica*: Dependence on the gene dosage, *Microbiology 142*, 1841−1846.

9. Nieto, J. M., Madrid, C., Miquelay, E., Parra, J. L., Rodriguez, S., and Juarez, A. (2002) Evidence for direct protein-protein interaction between members of the enterobacterial Hha/YmoA and H-NS families of proteins, *J. Bacteriol. 184*, 629−635.

10. Nieto, J. M., Madrid, C., Prenafeta, A., Miquelay, E., Balsalobre, C., Carrascal, M., and Juarez, A. (2000) Expression of the hemolysin operon in *Escherichia coli* is modulated by a nucleoid-protein complex that includes the proteins Hha and H-NS, *Mol. Gen. Genet. 263*, 349−358.

11. Tupper, A. E., Owen-Hughes, T. A., Ussery, D. W., Santos, D. S., Ferguson, D. J., Sidebotham, J. M., Hinton, J. C., and Higgins, C. F. (1994) The chromatin-associated protein H-NS alters DNA topology in vitro, *EMBO J. 13*, 258−268.

12. Dame, R. T., Wyman, C., and Goosen, N. (2000) H-NS mediated compaction of DNA visualised by atomic force microscopy, *Nucleic Acids Res. 28*, 3504−3510.

13. Schneider, R., Lurz, R., Luder, G., Tolksdorf, C., Travers, A., and Muskhelishvili, G. (2001) An architectural role of the *Escherichia coli* chromatin protein FIS in organising DNA, *Nucleic Acids Res. 29*, 5107−5114.

14. Spurio, R., Falconi, M., Brandi, A., Pon, C. L., and Gualerzi, C. O. (1997) The oligomeric structure of nucleoid protein H-NS is necessary for recognition of intrinsically curved DNA and for DNA bending, *EMBO J. 16*, 1795−1805.

15. Yamada, H., Yoshida, T., Tanaka, K., Sasakawa, C., and Mizuno, T. (1991) Molecular analysis of the *Escherichia coli* hns gene encoding a DNA-binding protein, which preferentially recognizes curved DNA sequences, *Mol. Gen. Genet. 230*, 332−336.

16. Bouffartigues, E., Buckle, M., Badaut, C., Travers, A., and Rimsky, S. (2007) H-NS cooperative binding to high-affinity sites in a regulatory element results in transcriptional silencing, *Nat. Struct. Mol. Biol. 14*, 441−448.

17. Smyth, C. P., Lundback, T., Renzoni, D., Sailigardi, G., Beavil, R., Layton, M., Sidebotham, J. M., Jay, C. D., Hinton, P. C., Driscoll, P. C., Higgins, C. F., and Ladbury, J. E. (2000) Oligomerization of the chromatin-structuring protein H-NS, *Mol. Microbiol. 36*, 962−972.

18. Ceschini, S., Lupidi, G., Coletta, M., Pon, C. L., Fioretti, E., and Angeletti, M. (2000) Multimeric self-assembly equilibria involving the histone-like protein H-NS. A thermodynamic study, *J. Biol. Chem. 275*, 729−734.

19. Dame, R. T., and Goosen, N. (2002) HU: Promoting or counteracting DNA compaction, *FEBS Lett. 529*, 151−156.

20. Williams, R. M., Rimsky, S., and Buc, H. (1996) Probing the structure, function, and interactions of the *Escherichia coli* H-NS and StpA proteins by using dominant negative derivatives, *J. Bacteriol. 178*, 4335−4343.

21. Ueguchi, C., Suzuki, T., Yoshida, T., Tanaka, K., and Mizuno, T. (1996) Systematic mutational analysis revealing the functional domain organization of *Escherichia coli* nucleoid protein H-NS, *J. Mol. Biol. 263*, 149−162.

22. Shindo, H., Iwaki, T., Ieda, R., Kurumizaka, H., Ueguchi, C., Mizuno, T., Morikawa, S., Nakamura, H., and Kuboniwa, H. (1995) Solution structure of the DNA binding domain of a nucleoid-associated protein, H-NS, from *Escherichia coli*, *FEBS Lett. 360*, 125−131.

23. Esposito, D., Petrovic, A., Harris, R., Ono, S., Eccleston, J. F., Mbabaali, A., Haq, I., Higgins, C. F., Hinton, J. C., Driscoll, P. C., and Ladbury, J. E. (2002) H-NS oligomerization domain structure reveals the mechanism for high order self-association of the intact protein, *J. Mol. Biol. 324*, 841−850.

24. Bloch, V., Yang, Y., Margeat, E., Chavanieu, A., Auge, M. T., Robert, B., Arold, S., Rimsky, S., and Kochoyan, M. (2003) The H-NS dimerization domain defines a new fold contributing to DNA recognition, *Nat. Struct. Biol. 10*, 212−218.

25. Garcia, J., Cordeiro, T. N., Nieto, J. M., Pons, I., Juarez, A., and Pons, M. (2005) Interaction between the bacterial nculeoid associated proteins Hha and H-NS involves a conformational change of Hha, *Biochem. J. 15*, 755−762.

26. Garcia, J., Madrid, C., Juarez, A., and Pons, M. (2006) New roles for key residues in helices H1 and H2 of the *Escherichia coli* H-NS N-terminal domain: H-NS dimer stabilization and Hha binding, *J. Mol. Biol. 359*, 679−689.

27. Rodriguez, S., Nieto, J. M., Madrid, C., and Juarez, A. (2005) Functional replacement of the oligomerization domain of H-NS by the Hha protein of *Escherichia coli*, *J. Bacteriol. 187*, 5452−5459.

28. Fox, J. D., and Waugh, D. S. (2003) Maltose-binding protein as a solubility enhancer, *Methods Mol. Biol. 205*, 99−117.

29. Kapust, R. B., and Waugh, D. S. (2000) Controlled intracellular processing of fusion proteins by TEV protease, *Protein Expression Purif. 19*, 312−318.

30. Sattler, M., Schleucher, J., and Griesinger, C. (1999) Heternuclear multidimensional NMR experiments for the structure determination of proteins in solution employing pulsed field gradients, *Prog. Nucl. Magn. Reson. Spectrosc. 34*, 93−158.

31. Yamazaki, T., Forman-Kay, J., and Kay, L. E. (1993) Two-Dimensional NMR Experiments for Correlating $^{13}C\beta$ and $^1H\delta/\epsilon$ Chemical Shifts of Aromatic Residues in ^{13}C-Labeled Proteins via Scalar Couplings, *J. Am. Chem. Soc. 115*, 11054−11055.

32. Meissner, A., and Sorensen, O. W. (2000) Suppression of diagonal peaks in three-dimensional protein NMR TROSY-type HCCH correlation experiments, *J. Magn. Reson. 144*, 171−174.

33. Meissner, A., and Sorensen, O. W. (1999) Optimization of three-dimensional TROSY-type HCCH NMR correlation of aromatic ^{1}H-^{13}C groups in proteins, *J. Magn. Reson. 139*, 447−450.

34. Kuboniwa, H., Grzesiek, S., Delaglio, F., and Bax, A. (1994) Measurement of HN-Hα J couplings in calcium-free calmodulin using new 2D and 3D water-flip-back methods, *J. Biomol. NMR 4*, 871−878.

35. McFeeters, R. L., Fowler, C. A., Gaponenko, V. V., and Byrd, R. A. (2005) Efficient and precise measurement of Hα-Cα, Cα-C′, Cα-Cβ, and HN-N residual dipolar couplings from 2D HN-N correlation spectra, *J. Biomol. NMR 31*, 35−47.

36. Sass, H. J., Musco, G., Stahl, S. J., Wingfield, P. T., and Grzesiek, S. (2000) Solution NMR of proteins within polyacrylamide gels: Diffusional properties and residual alignment by mechanical stress or embedding of oriented purple membranes, *J. Biomol. NMR 18*, 303−309.

37. Tycko, R., Blanco, F. J., and Ishii, Y. (2000) Alignment of biopolymers in strained gels: A new way to create detectable dipole-dipole couplings in high-resolution biomolecular NMR, *J. Am. Chem. Soc. 122*, 9340−9341.

38. Delaglio, F., Grzesiek, S., Vuister, G. W., Zhu, G., Pfeifer, J., and Bax, A. (1995) NMRPipe: A multidimensional spectral processing system based on UNIX pipes, *J. Biomol. NMR 6*, 277−293.

39. Goddard, T. D., and Kneller, D. G. (2005) *SPARKY 3*, University of California, San Francisco.

40. Tjandra, N., Feller, S. E., Pastor, R. W., and Bax, A. (1995) Rotational Diffusion Anisotropy of Human Ubiquitin from ^{15}N NMR Relaxation, *J. Am. Chem. Soc. 117*, 12562−12566.

41. Mandel, A. M., Akke, M., and Palmer, A. G., III (1996) Dynamics of ribonuclease H: Temperature dependence of motions on multiple time scales, *Biochemistry 35*, 16009−16023.

42. Cornilescu, G., Delaglio, F., and Bax, A. (1999) Protein backbone angle restraints from searching a database for chemical shift and sequence homology, *J. Biomol. NMR 13*, 289−302.

43. Schwieters, C. D., Kuszewski, J. J., Tjandra, N., and Clore, G. M. (2003) The Xplor-NIH NMR molecular structure determination package, *J. Magn. Reson. 160*, 65−73.

44. Yee, A., Chang, X., Pineda-Lucena, A., Wu, B., Semesi, A., Le, B., Ramelot, T., Lee, G. M., Bhattacharyya, S., Gutierrez, P., Denisov, A., Lee, C. H., Cort, J. R., Kozlov, G., Liao, J., Finak, G., Chen, L., Wishart, D., Lee, W., McIntosh, L. P., Gehring, K., Kennedy, M. A., Edwards, A. M., and Arrowsmith, C. H. (2002) An NMR approach to structural proteomics, *Proc. Natl. Acad. Sci. U.S.A. 99*, 1825−1830.

45. Schubert, M., Labudde, D., Oschkinat, H., and Schmieder, P. (2002) A software tool for the prediction of Xaa-Pro peptide bond conformations in proteins based on ^{13}C chemical shift statistics, *J. Biomol. NMR 24*, 149−154.

46. Ellison, D. W., Young, B., Nelson, K., and Miller, V. L. (2003) YmoA negatively regulates expression of invasin from *Yersinia enterocolitica*, *J. Bacteriol. 185*, 7153−7159.